

## **198516: pelitic granofels, Quajabin Peak**

### **(South West Terrane, Yilgarn Craton)**

**Blereau, ER, Korhonen, FJ, Fielding, IOH and Kelsey, DE**

### **Location and sampling**

CORRIGIN (SI 50-3), BROOKTON (2533)

MGA Zone 50, 517928E 6436376N

Warox Site FJKBGD198516

Sampled on 2 June 2010

This sample was collected from outcrop in a field on the north side of Yenyening Lakes Road, about 5.3 km northeast of Qualandary Pool, 2.2 km north of the Yenyening Lakes Nature Reserve and 1.7 km southeast of Quajabin Peak. The sample was collected as part of the Yilgarn Craton Metamorphic Project (2003–14) undertaken by Ben Goscombe for the Geological Survey of Western Australia (GSWA), and referred to in that study as sample BG10-8b. The results from this project have not been released by GSWA, although select data have been published in Goscombe et al. (2019).

### **Geological context**

The unit sampled is a granulite-grade pelitic granofels near the eastern margin of the South West Terrane (Quentin de Gromard et al., 2021). The unit is part of a northwest-trending belt of Archean metasedimentary and gneissic rocks referred to by Wilde (2001) and Bosch et al. (1996) as the Jimperding metamorphic belt. The boundary between the South West and Youanmi Terranes in this area is a major, northwest-trending shear zone system (Quentin de Gromard et al., 2021). Four quartzite samples, collected between 88 and 99 km northwest of this locality, yielded detrital zircon ages between c. 3700 and 3000 Ma, and maximum ages of deposition between c. 3203 and 3005 Ma (GSWA 177901, Wingate et al., 2008a; GSWA 177904, Wingate et al., 2008b; GSWA 177907, Wingate et al., 2008c; GSWA 177908, Wingate et al., 2008d; Pidgeon et al., 2010). Zircon rims in two of these samples have been interpreted to date amphibolite facies metamorphism at c. 2660 Ma (GSWA 177907, Wingate et al., 2008c; GSWA 177908, Wingate et al., 2008d). Two samples of Fe-rich pelitic granofels collected about 21 km to the east-northeast, within the Youanmi Terrane, yielded weighted mean  $^{207}\text{Pb}/^{206}\text{Pb}$  monazite dates of  $2651 \pm 6$  and  $2656 \pm 6$  Ma, interpreted as the ages of high-grade metamorphism (GSWA 198520, Fielding et al., 2021a; GSWA 198522, Fielding et al., 2021b). Monazite from the sample reported here yielded a weighted mean  $^{207}\text{Pb}/^{206}\text{Pb}$  date of  $2647 \pm 5$  Ma, interpreted as the age of high-grade metamorphism (GSWA 198516, Fielding et al., 2021c).

### **Petrographic description**

The sample is an unfoliated, fine- to medium-grained pelitic gneiss, consisting of about 44% quartz, 28% cordierite, 16% biotite, 7% plagioclase, 3% garnet, 1% fibrolitic sillimanite, 1% muscovite, minor ilmenite and Cr-bearing spinel, and trace amounts of zircon and monazite (Fig. 1; Table 1). Quartz in the matrix is anhedral, up to 5 mm in size, and exhibits undulose extinction. Cordierite is Fe-rich ( $X_{\text{Fe}} = 0.40\text{--}0.41$ ; Table 2) and occurs as partially pinitized porphyroblastic grains in the matrix that are 1–3 mm in size and as moats intergrown with biotite surrounding garnet (Fig. 2). Biotite occurs as discrete red-brown laths up to 3 mm long mantling cordierite and garnet, and also occurs as a symplectic intergrowth with quartz and cordierite around garnet (Figs 1, 2) that is interpreted to be related to partial melting. Plagioclase in the matrix is subhedral, 0.5–2 mm in size, and is variably replaced by sericite. Equant anhedral garnet porphyroblasts range in size 1–3 mm and contain rounded quartz inclusions (Figs 1, 2). Small rounded to embayed garnet grains are partly to fully mantled by cordierite (Figs 1, 2a). Garnet porphyroblasts are almandine-rich ( $X_{\text{Fe}} = 0.80\text{--}0.90$ ; Table 2), with a slight decrease in Mg and increase in Mn from core to rim (Table 2; Appendix 1). Fibrolite occurs as yellow matted aggregates up to 2 mm in size that are

intergrown with biotite near cordierite and quartz (Fig. 2a). Muscovite occurs as laths up to 1 mm in size within the matrix and as sericite replacing plagioclase, interpreted to be retrograde. Ilmenite and Cr-bearing spinel are closely associated, occurring as discrete grains in the matrix up to 0.5 mm in diameter. This granulite facies granofels was likely derived from a pelitic metasedimentary protolith.

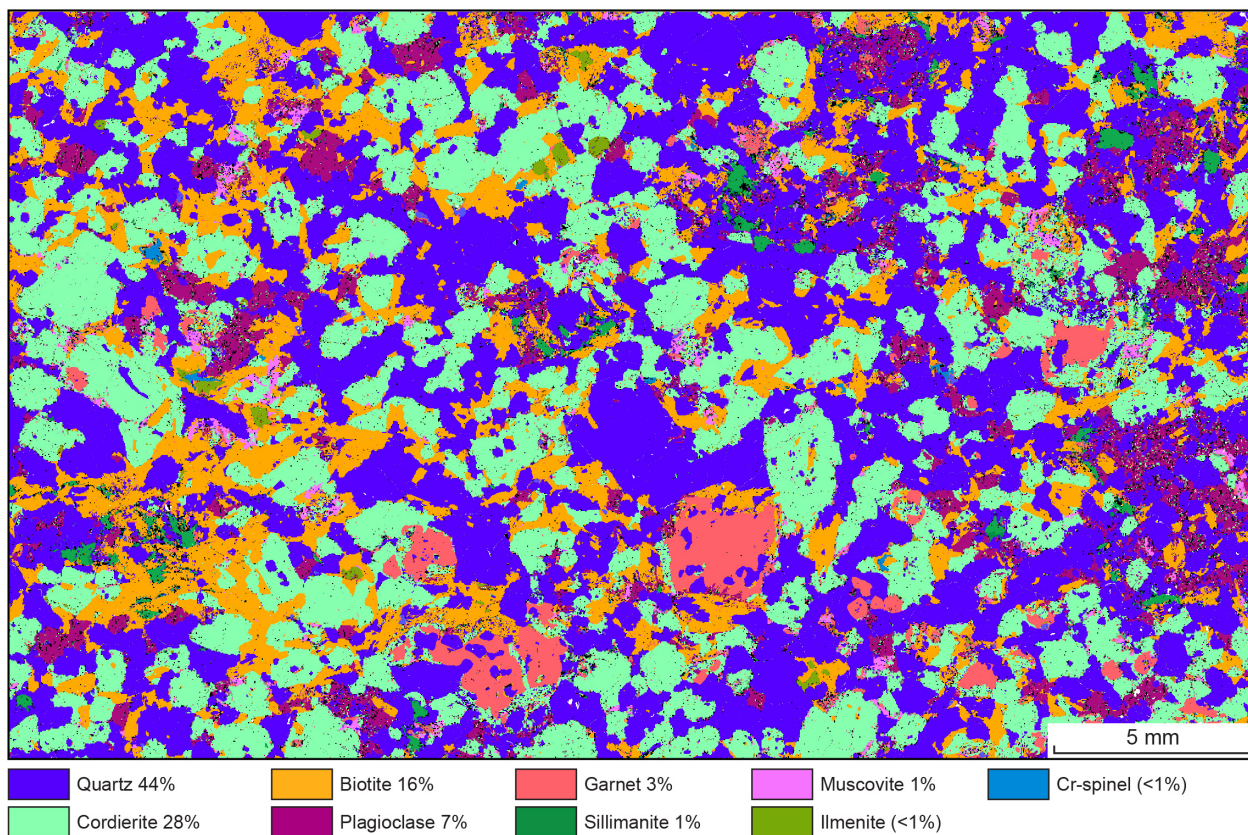


**Figure 1.** TESCAN Integrated Mineral Analyser (TIMA) image of an entire thin section from sample 198516: pelitic granofels, Quajabin Peak. Volume percent proportion of major rock-forming minerals are calculated by the TIMA software

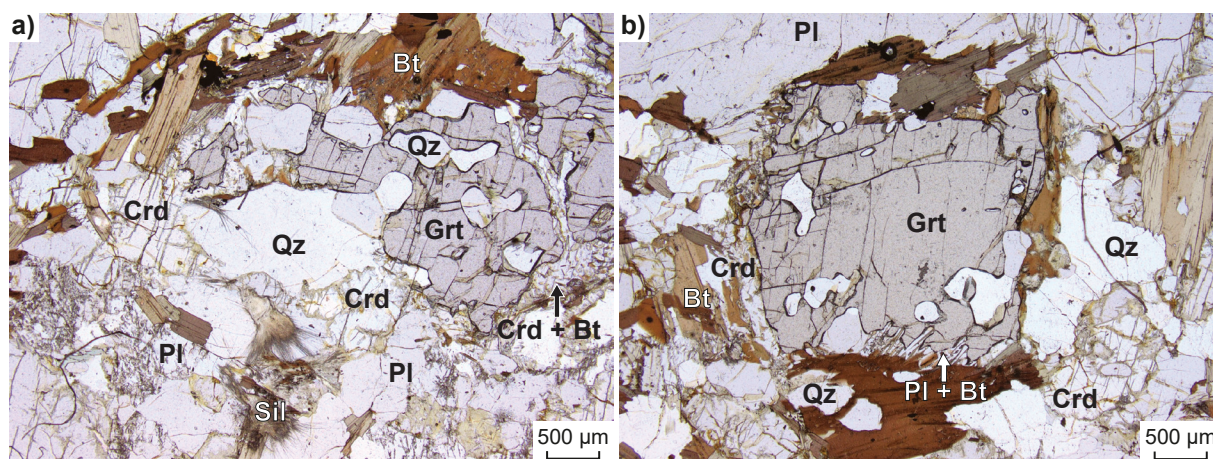


**Figure 2.** Photomicrographs, in plane polarized light, of sample 198516: pelitic granofels, Quajabin Peak. Mineral abbreviations are explained in the caption to Figure 3

**Table 1. Mineral modes for sample 198516: pelitic granulites, Quajabin Peak**

Mineral modes	Grt	Sil	Crd	Bt	Pl	Qz	Ilm	Mag	Liq
Observed (vol%)(a)	3	1	28	16	7	44	<1	–	–
Predicted (mol%)									
@ 890 °C, 4.1 kbar	0.1	3	25	13	9	38	0.6	0.5	9
@ 890 °C, 6.2 kbar	8	10	7	15	8	42	0.7	trace	11

NOTES: (a) 1% muscovite, minor Cr-bearing spinel, trace monzite and zircon also present in thin section  
– not present

## Analytical details

Preliminary  $P$ – $T$  estimates were obtained using multiple-reaction thermobarometry calculated from the mineral compositions (Table 2; Goscombe et al., 2019). These estimates were derived from the ‘averagePT’ module (avPT) in the program THERMOCALC version tc325 (Powell and Holland, 1988), using the internally consistent Holland and Powell (1998) dataset.

The metamorphic evolution of this sample was investigated using phase equilibria modelling, based on the bulk-rock composition (Table 3). The bulk-rock composition was determined by X-ray fluorescence spectroscopy, together with loss on ignition (LOI). FeO content was analysed by  $\text{Fe}^{2+}$  titration, and  $\text{Fe}_2\text{O}_3$  calculated by difference. The modelled O content (for  $\text{Fe}^{3+}$ ) was derived from the titration value; the modelled  $\text{H}_2\text{O}$  content was the measured LOI. The bulk composition was adjusted for the presence of apatite by applying a correction to CaO (Table 3). Thermodynamic calculations were performed in the MnNCKFMASHTO ( $\text{MnO}$ – $\text{Na}_2\text{O}$ – $\text{CaO}$ – $\text{K}_2\text{O}$ – $\text{FeO}$ – $\text{MgO}$ – $\text{Al}_2\text{O}_3$ – $\text{SiO}_2$ – $\text{H}_2\text{O}$ – $\text{TiO}_2$ – $\text{O}$ ) system using THERMOCALC version tc340 (Powell and Holland 1988; updated October 2013) and the internally consistent thermodynamic dataset of Holland and Powell (2011; dataset tc-ds62, created in February 2012). The activity–composition relations used in the modelling are detailed in White et al. (2014a,b). Compositional and mode isopleths for all phases were calculated using the software TCInvestigator (Pearce et al., 2015). Additional information on the workflow with relevant background and methodology are provided in Korhonen et al. (2020).



**Table 2. Mineral compositions for sample 198516: pelitic granofels, Quajabin Peak**

Mineral <sup>(a)</sup> Setting <sup>(b)</sup>	Crd Core	Crd Rim	Grt Core	Grt Rim	Grt OR	Crd MCore	Crd MRim	Bt Moat	Bt Core	Bt Rim	Sp Core	Ilm Core	Pl Core	Pl Rim	Ms LCore	Ms LRim
<i>wt%</i>																
SiO <sub>2</sub>	48.71	48.41	38.17	37.13	37.14	48.14	48.57	34.59	34.89	35.17	0.04	0.01	57.63	57.08	46.91	46.49
TiO <sub>2</sub>	0.00	0.00	0.02	0.02	0.01	0.02	0.00	1.77	2.28	2.73	0.10	52.14	0.00	0.02	0.59	0.45
Al <sub>2</sub> O <sub>3</sub>	31.53	31.43	21.09	20.79	20.59	31.38	31.62	19.16	18.65	18.85	43.48	0.00	25.63	25.63	36.76	37.04
Cr <sub>2</sub> O <sub>3</sub>	0.00	0.02	0.07	0.11	0.09	0.00	0.01	1.49	0.88	0.93	13.88	0.15	0.00	0.00	0.05	0.31
FeO	9.07	9.13	33.29	33.36	33.68	9.14	9.31	19.71	20.54	20.63	36.20	43.82	0.03	0.07	1.28	1.38
MnO	0.08	0.14	1.35	4.21	4.47	0.31	0.31	0.10	0.07	0.07	0.36	1.61	0.04	0.04	0.01	0.03
MgO	7.64	7.70	4.69	2.20	2.01	7.54	7.51	7.84	7.75	7.70	1.45	0.04	0.00	0.01	0.45	0.41
ZnO	0.00	0.00	0.07	0.10	0.13	0.00	0.00	0.00	0.00	0.06	2.74	0.00	0.03	0.01	0.02	0.03
CaO	0.03	0.03	1.39	1.45	1.44	0.03	0.02	0.03	0.00	0.00	0.02	0.03	8.48	8.48	0.00	0.00
Na <sub>2</sub> O	0.13	0.14	0.01	0.02	0.03	0.14	0.13	0.21	0.18	0.22	0.12	0.00	6.83	6.85	0.77	0.69
K <sub>2</sub> O	0.00	0.01	0.00	0.01	0.00	0.00	0.00	8.99	8.97	8.90	0.00	0.02	0.14	0.12	9.79	9.66
Total <sup>(c)</sup>	97.19	97.02	100.16	99.39	99.59	96.69	97.49	93.89	94.22	95.25	98.38	97.81	98.83	98.30	96.65	96.50
Oxygen	18	18	12	12	12	18	18	11	11	11	4	3	8	8	11	11
Si	5.09	5.07	3.03	3.03	3.03	5.06	5.07	2.68	2.70	2.69	0.00	0.00	2.61	2.60	3.08	3.06
Ti	0.00	0.00	0.00	0.00	0.00	0.00	0.00	0.10	0.13	0.16	0.00	1.01	0.00	0.00	0.03	0.02
Al	3.89	3.88	1.98	2.00	1.98	3.89	3.89	1.75	1.70	1.70	1.58	0.00	1.37	1.37	2.85	2.88
Cr	0.00	0.00	0.00	0.01	0.01	0.00	0.00	0.09	0.05	0.06	0.34	0.00	0.00	0.00	0.00	0.02
Fe <sup>3+(d)</sup>	0.00	0.01	0.00	0.00	0.00	0.01	0.00	0.06	0.07	0.07	0.08	0.00	0.00	0.00	0.00	0.00
Fe <sup>2+</sup>	0.79	0.79	2.21	2.27	2.30	0.79	0.81	1.21	1.26	1.25	0.85	0.95	0.00	0.00	0.07	0.08
Mn <sup>2+</sup>	0.01	0.01	0.09	0.29	0.31	0.03	0.03	0.01	0.00	0.00	0.01	0.04	0.00	0.00	0.00	0.00
Mg	1.19	1.20	0.56	0.27	0.24	1.18	1.17	0.90	0.89	0.88	0.07	0.00	0.00	0.00	0.04	0.04
Zn	0.00	0.00	0.00	0.01	0.01	0.00	0.00	0.00	0.00	0.00	0.06	0.00	0.00	0.00	0.00	0.00
Ca	0.00	0.00	0.12	0.13	0.13	0.00	0.00	0.00	0.00	0.00	0.00	0.00	0.41	0.41	0.00	0.00
Na	0.03	0.03	0.00	0.00	0.00	0.03	0.03	0.03	0.03	0.03	0.01	0.00	0.60	0.60	0.10	0.09
K	0.00	0.00	0.00	0.00	0.00	0.00	0.00	0.89	0.88	0.87	0.00	0.00	0.01	0.01	0.82	0.81
Total	11.00	11.00	8.00	8.00	8.00	11.00	11.00	7.73	7.72	7.70	3.00	2.00	5.00	5.00	7.00	7.00
<i>Compositional variables</i>																
XFe <sup>(e)</sup>	0.40	0.40	0.80	0.89	0.90	0.40	0.41	0.57	0.59	0.59	0.93	1.00	–	–	0.61	0.66

**NOTES:** – not applicable  
(a) Mineral abbreviations explained in the caption to Figure 3  
(b) OR, outer rim; MCore, moat (core) around garnet; MRim, moat (rim) around garnet; LCore/LRim, Late core/rim  
(c) Totals on anhydrous basis  
(d) Fe<sup>3+</sup> contents for biotite assumed to be 10% of Fe total; Fe<sup>3+</sup> contents for other minerals based on Droop (1987)  
(e) XFe = Fe<sup>2+</sup>/(Fe<sup>2+</sup> + Mg)

**Table 3. Measured whole-rock and modelled compositions for sample 198516: pelitic granofels, Quajabin Peak**

<i>XRF whole-rock composition (wt%)<sup>(a)</sup></i>												
SiO <sub>2</sub>	TiO <sub>2</sub>	Al <sub>2</sub> O <sub>3</sub>	Fe <sub>2</sub> O <sub>3</sub> <sup>(b)</sup>	FeO <sup>(b)</sup>	MnO	MgO	CaO	Na <sub>2</sub> O	K <sub>2</sub> O	P <sub>2</sub> O <sub>5</sub>	LOI	Total
66.69	0.66	16.45	1.01	6.27	0.13	2.93	0.93	0.86	1.83	0.02	1.49	99.27
<i>Normalized composition used for phase equilibria modelling (mol%)</i>												
SiO <sub>2</sub>	TiO <sub>2</sub>	Al <sub>2</sub> O <sub>3</sub>	O <sup>(c)</sup>	FeO <sup>T(d)</sup>	MnO	MgO	CaO <sup>(e)</sup>	Na <sub>2</sub> O	K <sub>2</sub> O	--	H <sub>2</sub> O <sup>(f)</sup>	Total
69.71	0.52	10.13	0.39	6.27	0.12	4.57	1.01	0.87	1.22	–	5.19	100

**NOTES:** (a) Data and analytical details are available from the WACHEM database <<http://geochem.dmp.wa.gov.au/geochem/>>  
(b) FeO analysed by Fe<sup>2+</sup> titration; Fe<sub>2</sub>O<sub>3</sub> content calculated by difference  
(c) O content (for Fe<sub>2</sub>O<sub>3</sub>) derived from the titration value  
(d) CaO modified to remove apatite: CaO(Mod) = CaO(Total) - (moles CaO(in Ap) = 3.33 \* moles P<sub>2</sub>O<sub>5</sub>)  
(e) H<sub>2</sub>O content is the measured LOI  
– not applicable



## Results

Metamorphic  $P$ – $T$  estimates have been derived based on detailed examination of one thin section and the bulk-rock composition; care was taken to ensure that the thin section and the sample volume selected for whole-rock chemistry were similar in terms of featuring the same minerals in approximately the same abundances (Table 1), to minimize any potential compositional differences. The  $P$ – $T$  pseudosection was calculated over a  $P$ – $T$  range of 3–8 kbar and 600–900 °C (Fig. 3). The  $H_2O$ -saturated solidus is located between 685 and 705 °C across the modelled pressure range. Garnet has a wide stability; garnet-absent assemblages are only predicted below 4 kbar between 600 and 760 °C. Chlorite is stable at the lowest temperatures across the range of modelled pressures, followed by staurolite, and sillimanite with increasing temperature. Aluminosilicate minerals, mainly sillimanite, are stable over most of the range of modelled conditions, except at lower temperatures where staurolite is stable, and at low- $P$ /high- $T$  conditions. Magnetite is stable below 600 °C at 4.8 kbar and below 5.6 kbar at 705 °C. Cordierite is stable across the range of modelled temperatures, below 4.2 kbar at 600 °C and 7.05 kbar at 850 °C. Orthopyroxene is stable below 3.5 kbar and above 795 °C.

Metamorphic  $P$ – $T$  estimates ( $\pm 2\sigma$  uncertainty) calculated using multiple-reaction thermobarometry are  $7.1 \pm 1.05$  kbar and  $798 \pm 71$  °C (Goscombe et al., 2019). These calculations used the core compositions (Table 2) to estimate peak conditions.

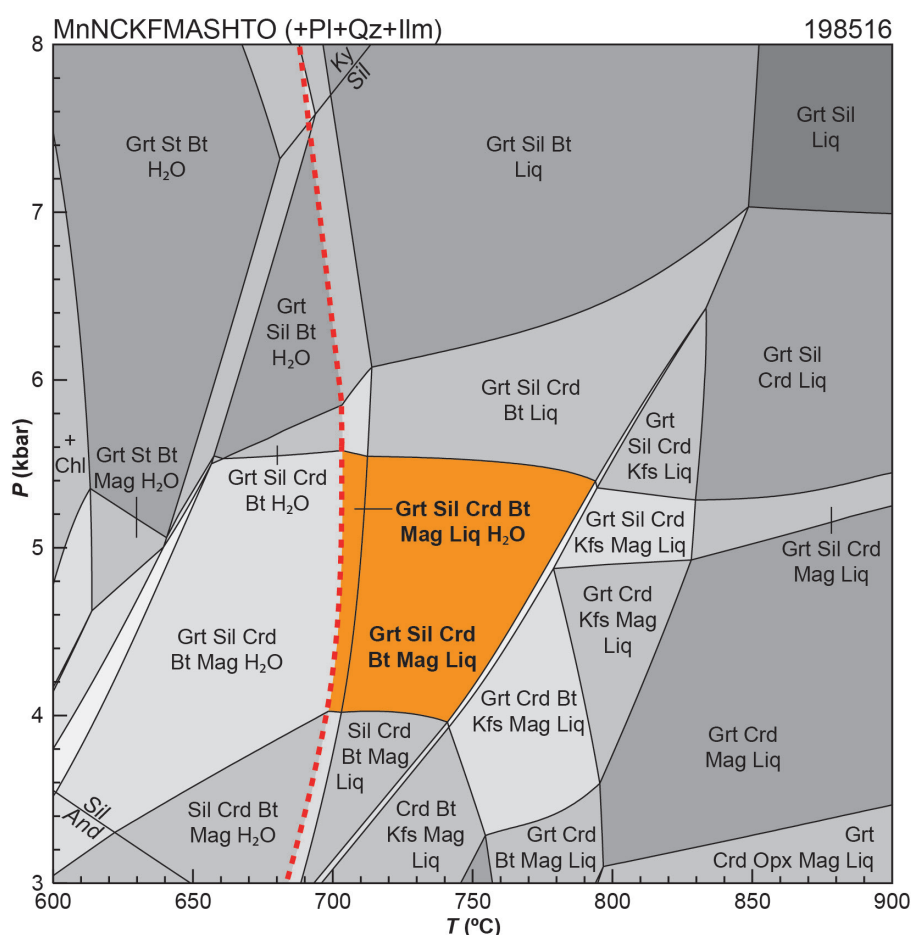


**Figure 3.**  $P$ – $T$  pseudosection calculated for sample 198516: pelitic granofels, Quajabin Peak. Assemblage fields corresponding to peak metamorphic conditions are shown in bold text and orange shading. Red dashed line represents the solidus. Abbreviations: And, andalusite; Bt, biotite; Chl, chlorite; Crd, cordierite; Grt, garnet;  $H_2O$ , fluid (pure  $H_2O$ ); Ilm, ilmenite; Kfs, K-feldspar; Ky, kyanite; Liq, silicate melt; Mag, magnetite; Opx, orthopyroxene; Pl, plagioclase; Qz, quartz; Sil, sillimanite; St, staurolite

## Interpretation

Based on the coarser grain size and mineral associations that support textural equilibrium, the peak granulite-grade metamorphic assemblage is interpreted to contain garnet, cordierite, plagioclase, quartz, ilmenite, Cr-rich spinel and melt. The rims of garnet porphyroblasts are interpreted to be part of the peak metamorphic assemblage, and the growth of the cores occurred during prograde metamorphism. Biotite that is in textural equilibrium with cordierite in the matrix could have been part of the peak metamorphic assemblage, although biotite rims on garnet porphyroblasts are interpreted to post-date garnet growth. Porphyroblastic cordierite is interpreted to have been stable during peak- to post-peak metamorphism, whereas cordierite mantling garnet is interpreted to replace and thus post-date garnet growth. Mn-rich garnet rims support that garnet has been partly resorbed during growth of another mineral, possibly cordierite and/or biotite. Sillimanite is inferred to have been part of the peak assemblage, although some fibrolite intergrown with biotite likely occurred on the retrograde  $P$ – $T$  path.

The inferred peak assemblage is garnet–sillimanite–cordierite–biotite–plagioclase–quartz–ilmenite–melt. The trace amount of spinel observed in the thin section is not further considered due to the significant amount of Cr (Table 2), which cannot be modelled in the MnNCKFMASHTO system. The predicted mineral modes (molar proportions approximately equivalent to vol%) across garnet–cordierite–biotite-bearing fields at 725 °C are most consistent with inclusion of magnetite as a peak mineral (Table 1; Fig. 4). Magnetite is not observed in the thin section, although predicted modes are  $<1$  mol% (Table 1). At pressures above 5.6 kbar, magnetite is no longer stable, but the predicted modes of garnet, sillimanite and cordierite are significantly different to the modes observed in the thin section (Table 1; Fig. 4). Based on these constraints, the peak assemblage is interpreted to be garnet–sillimanite–cordierite–biotite–plagioclase–quartz–ilmenite–magnetite–melt( $\text{H}_2\text{O}$ ), which is stable between 695 and 795 °C at 4.0 – 5.6 kbar. This peak field is delimited by the loss of garnet at lower pressure, loss of magnetite at higher pressure, growth of K-feldspar at higher temperature, and the crystallization of melt at lower temperatures. Mineral compositions suggest equilibration at  $798 \pm 71$  °C,  $7.1 \pm 1.05$  kbar, although Goscombe et al. (2019) acknowledge that this pressure may be overestimated and offer an alternative result of 790 °C and 6 kbar based on the upper pressure limit of the peak assemblage on a published  $P$ – $T$  pseudosection. However, the pseudosection used by Goscombe et al. (2019) has a more Mg-rich bulk composition than the sample reported here, so these results have significant uncertainty. The compositions of garnet ( $X_{\text{Fe}} = 0.80 - 0.90$ ) and cordierite ( $X_{\text{Fe}} = 0.40 - 0.41$ ) porphyroblasts broadly support final equilibration near the lower pressure limit of the peak field at the solidus (Appendix 2). Cordierite growth at the expense of garnet also requires a decrease in pressure within the peak field (Fig. 4a,b), followed by a small increase in sillimanite and biotite (Fig. 4c,d) during cooling to conditions below the solidus. These constraints indicate a clockwise retrograde trajectory within the peak field to final melt crystallization at about 4 kbar and 700 °C.

Peak metamorphic conditions are estimated at 695–795 °C and 4.0 – 5.6 kbar, with an apparent thermal gradient between 125 and 185 °C/kbar. The growth of cordierite after garnet, and retrograde growth of sillimanite and biotite broadly support a clockwise retrograde path with final melt crystallization at about 4 kbar and 700 °C, defining a thermal gradient of 175 °C/kbar.

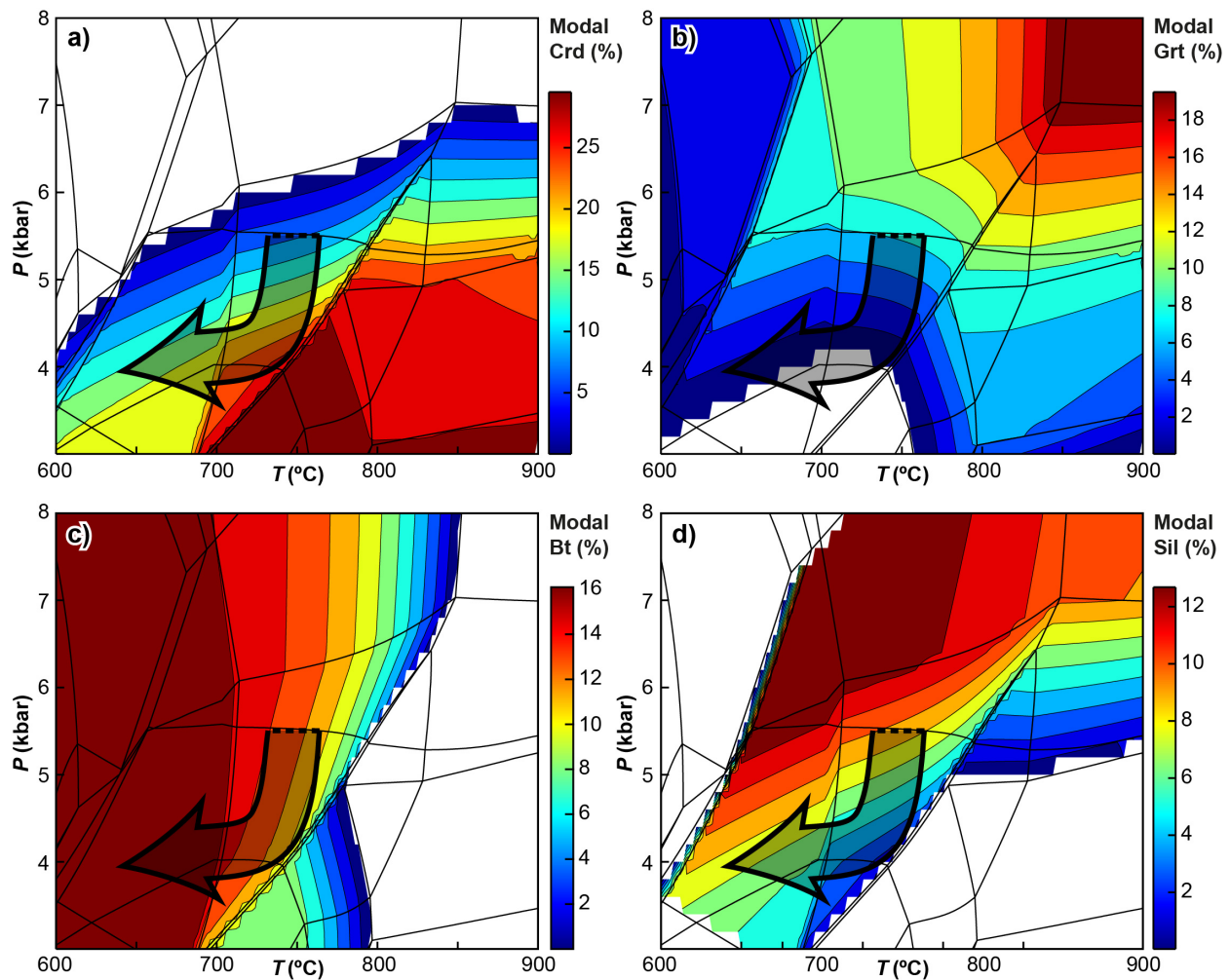


**Figure 4.** Mode isopleths (mineral proportions; approximately equal to volume percent) for selected minerals in sample 198516: pelitic granulites, Quajabin Peak (see Figure 3 for labelled  $P$ – $T$  diagram). The growth of cordierite after garnet, and retrograde growth of sillimanite and biotite broadly support a clockwise trajectory; schematic  $P$ – $T$  path is represented by the grey arrow, with thickness of the arrow to qualitatively depict uncertainty

## References

- Bosch, D, Bruguier, O and Pidgeon, RT 1996, Evolution of an Archean metamorphic belt: A conventional and SHRIMP U–Pb study of accessory minerals from the Jimperding metamorphic belt, Yilgarn Craton, Western Australia: *The Journal of Geology*, v. 104, p. 695–711.
- Droop, GTR 1987, A general equation for estimating  $\text{Fe}^{3+}$  concentrations in ferromagnesian silicates and oxides from microprobe analyses, using stoichiometric criteria: *Mineralogical Magazine*, v. 51, no. 361, p. 431–435.
- Fielding, IOH, Wingate, MTD, Korhonen, FJ and Rankenburg, K 2021a, 198520: pelitic granulites, Tregenza Road; *Geochronology Record 1765*: Geological Survey of Western Australia, 5p.
- Fielding, IOH, Wingate, MTD, Korhonen, FJ and Rankenburg, K, 2021b; 198522: pelitic granulites, Tregenza Road; *Geochron Record 1766*: Geological Survey of Western Australia, 5p.
- Fielding, IOH, Wingate, MTD, Korhonen, FJ and Rankenburg, K 2021c, 198516: pelitic granulites, Quajabin Peak; *Geochronology Record 1764*: Geological Survey of Western Australia, 5p.
- Goscombe, B, Foster, DA, Blewett, R, Czarnota, K, Wade, B, Groenewald, B and Gray, D 2019, Neoarchaeon metamorphic evolution of the Yilgarn Craton: a record of subduction, accretion, extension and lithospheric delamination: *Precambrian Research*, article no. 105441, doi:10.1016/j.precamres.2019.105441.
- Holland, TJB and Powell, R 2011, An improved and extended internally consistent thermodynamic dataset for phases of petrological interest, involving a new equation of state for solids: *Journal of Metamorphic Geology*, v. 29, no. 3, p. 333–383.
- Korhonen, FJ, Kelsey, DE, Fielding, IOH and Romano, SS 2020, The utility of the metamorphic rock record: constraining the pressure–temperature–time conditions of metamorphism: *Geological Survey of Western Australia, Record 2020/14*, 24p.
- Pearce, MA, White, AJR and Gazley, MF 2015, TCInvestigator: automated calculation of mineral mode and composition contours for thermocalc pseudosections: *Journal of Metamorphic Geology*, v. 33, no. 4, p. 413–425, doi:10.1111/jmg.12126.
- Pidgeon, RT, Wingate, MTD, Bodorkos, S and Nelson, DR 2010, The age distribution of detrital zircons in quartzites from the Toodyay – Lake Grace Domain, Western Australia: implications for the early evolution of the Yilgarn Craton: *American Journal of Science*, v. 310, p. 1115–1135.



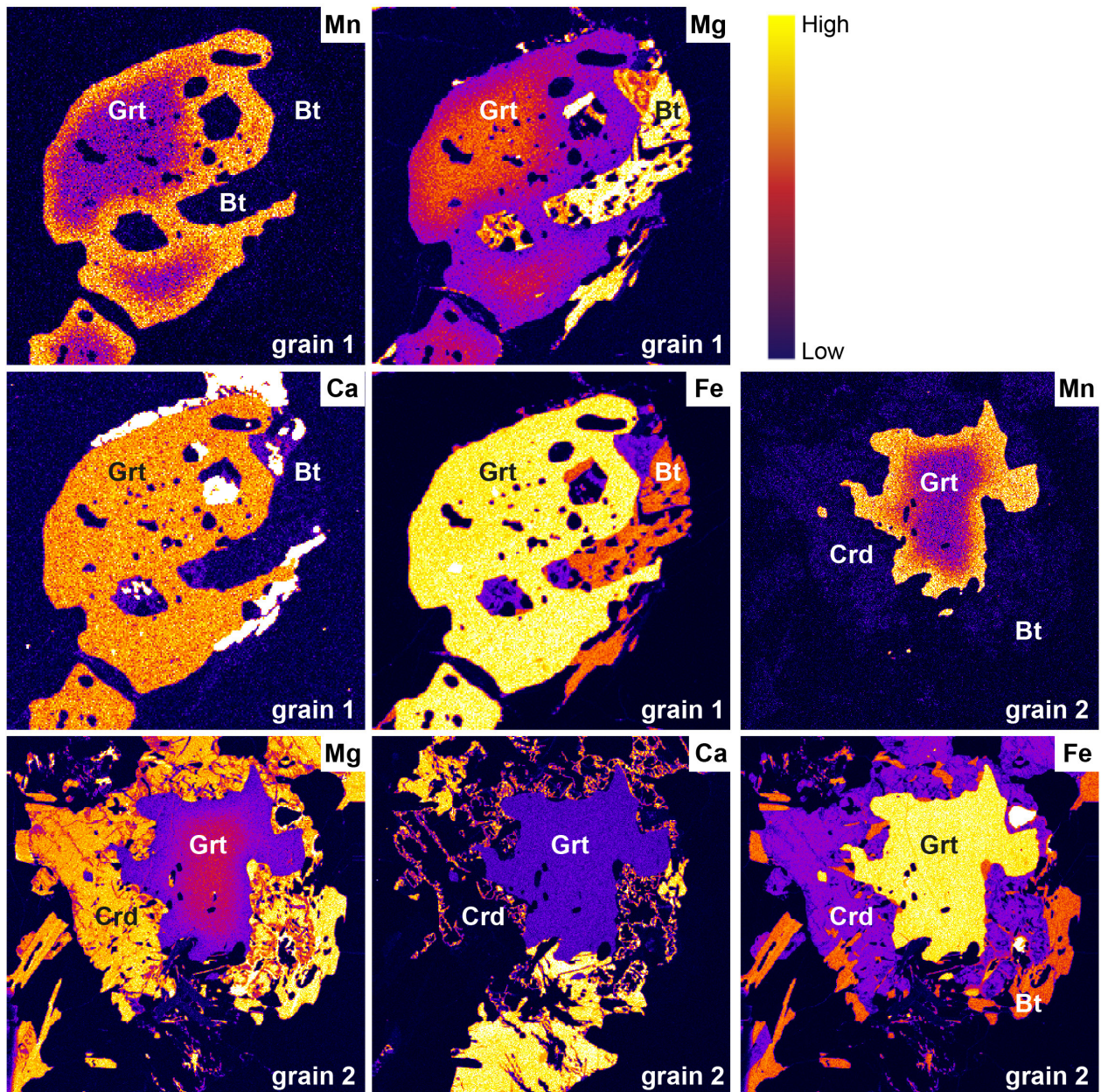
- Powell, R and Holland, TJB 1988, An internally consistent dataset with uncertainties and correlations: 3. Applications to geobarometry, worked examples and a computer program: *Journal of Metamorphic Geology*, v. 6, no. 2, p. 173–204.
- Quentin de Gromard, R, Ivanic, TJ and Zibra, I 2021, Interpreted bedrock geology of the southwest Yilgarn Craton, Geological Survey of Western Australia, in press.
- White, RW, Powell, R, Holland, TJB, Johnson, TE and Green, ECR 2014a, New mineral activity-composition relations for thermodynamic calculations in metapelitic systems: *Journal of Metamorphic Geology*, v. 32, no. 3, p. 261–286.
- White, RW, Powell, R and Johnson, TE 2014b, The effect of Mn on mineral stability in metapelites revisited: New a-x relations for manganese-bearing minerals: *Journal of Metamorphic Geology*, doi:10.1111/jmg.12095.
- Wilde, SA 2001, Jimperding and Chittering metamorphic belts, Western Australia — a field guide: Geological Survey of Western Australia, Record 2001/12, 24p.
- Wingate, MTD, Bodorkos, S, and Kirkland, CL 2008a, 177901: quartzite, Kowalyou; Geochronology Record 739: Geological Survey of Western Australia, 5p.
- Wingate, MTD, Bodorkos, S, and Kirkland, CL 2008b, 177904: quartzite, Windmill Hill; Geochronology Record 740: Geological Survey of Western Australia, 7p.
- Wingate, MTD, Bodorkos, S, and Kirkland, CL 2008c, 177907: quartzite, Noondeening Hill; Geochronology Record 741: Geological Survey of Western Australia, 7p.
- Wingate, MTD, Bodorkos, S, and Kirkland, CL 2008d, 177908: quartzite, Noondeening Hill; Geochronology Record 742: Geological Survey of Western Australia, 7p.

## Links

Metamorphic history introduction document: [Intro\\_2020.pdf](#)

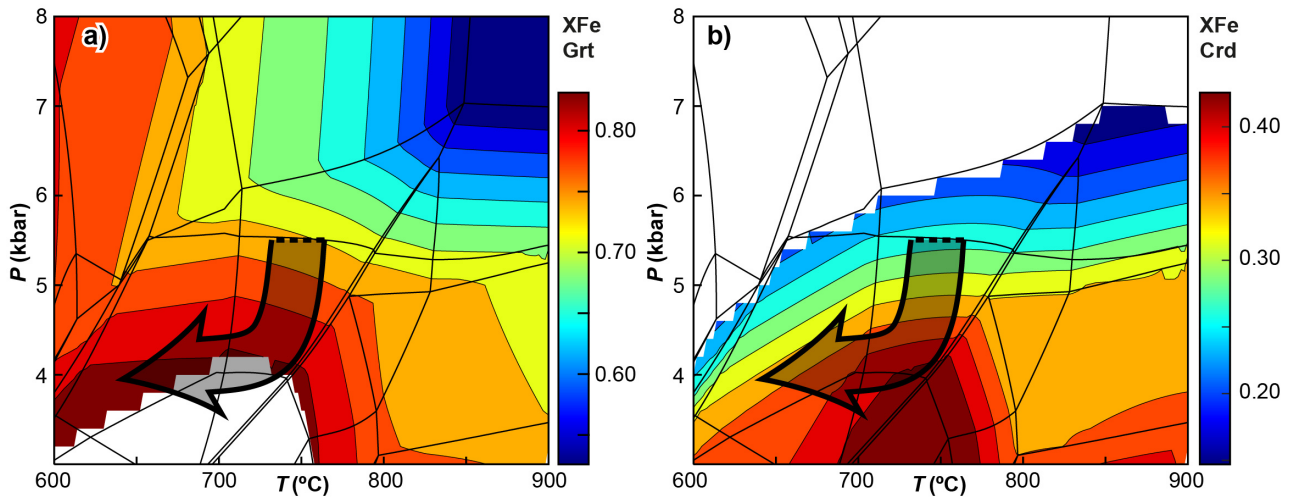
## Appendix 1

EPMA compositional maps of garnet from sample 198516: pelitic gneiss, Quajabin Peak. Maps were analysed by energy-dispersive spectroscopy, and show relative elemental abundances. These garnet porphyroblasts were analysed from a thin section of the sample that is not part of the GSWA collection, and as such there is no information on mineral size or petrographic context



## Appendix 2

Compositional isopleths of  $X_{Fe} (= Fe^{2+}/(Fe^{2+} + Mg))$  for selected minerals in sample 198516: pelitic granofels, Quajabin Peak (see Figure 3 for labelled  $P$ – $T$  diagram): a) garnet; b) cordierite. Schematic  $P$ – $T$  path is represented by the grey arrow, with thickness of the arrow to qualitatively depict uncertainty



### Recommended reference for this publication

Blereau, ER, Korhonen, FJ, Fielding, IOH and Kelsey, DE 2021, 198516: pelitic gneiss, Quajabin Peak; Metamorphic History Record 3: Geological Survey of Western Australia, 11p.

Data obtained: 10 September 2020

Date released: 25 June 2021

This Metamorphic History Record was last modified on 9 June 2021.

Grid references in this publication refer to the Geocentric Datum of Australia 1994 (GDA94). All locations are quoted to at least the nearest 100 m.

WAROX is GSWA's field observation and sample database. WAROX site IDs have the format 'ABCXXXnnnnnnSS', where ABC = geologist username, XXX = project or map code, nnnnnn = 6 digit site number, and SS = optional alphabetic suffix (maximum 2 characters).

Isotope and element analyses are routinely conducted using the GeoHistory laser ablation ICP-MS and Sensitive High-Resolution Ion Microprobe (SHRIMP) ion microprobe facilities at the John de Laeter Centre (JdLC), Curtin University, with the financial support of the Australian Research Council and AuScope National Collaborative Research Infrastructure Strategy (NCRIS). The TESCAN Integrated Mineral Analyser (TIMA) instrument was funded by a grant from the Australian Research Council (LE140100150) and is operated by the JdLC with the support of the Geological Survey of Western Australia, The University of Western Australia (UWA) and Murdoch University. Mineral analyses are routinely obtained using the electron probe microanalyser (EPMA) facilities at the Centre for Microscopy, Characterisation and Analysis at UWA, and at Adelaide Microscopy, University of Adelaide.

Digital data related to WA Geology Online, including geochronology and digital geology, are available online at the Department's [Data and Software Centre](#) and may be viewed in map context at [GeoVIEW.WA](#).

### Disclaimer

This product uses information from various sources. The Department of Mines, Industry Regulation and Safety (DMIRS) and the State cannot guarantee the accuracy, currency or completeness of the information. Neither the department nor the State of Western Australia nor any employee or agent of the department shall be responsible or liable for any loss, damage or injury arising from the use of or reliance on any information, data or advice (including incomplete, out of date, incorrect, inaccurate or misleading information, data or advice) expressed or implied in, or coming from, this publication or incorporated into it by reference, by any person whatsoever.





© State of Western Australia (Department of Mines, Industry Regulation and Safety) 2021

With the exception of the Western Australian Coat of Arms and other logos, and where otherwise noted, these data are provided under a Creative Commons Attribution 4.0 International Licence. (<http://creativecommons.org/licenses/by/4.0/legalcode>)

**Further details of geoscience products are available from:**

Information Centre

Department of Mines, Industry Regulation and Safety

100 Plain Street

EAST PERTH WA 6004

Telephone: +61 8 9222 3459 | Email: [publications@dmirs.wa.gov.au](mailto:publications@dmirs.wa.gov.au)

[www.dmirs.wa.gov.au/GSWApublications](http://www.dmirs.wa.gov.au/GSWApublications)